JOURNAL OF CHEMICAL INFORMATION AND MODELING

Article

pubs.acs.org/jcim

Enhancing the Sensitivity of Pharmacophore-Based Virtual Screening by Incorporating Customized ZBG Features: A Case Study Using Histone Deacetylase 8

Xuben Hou,[†] Jintong Du,[‡] Renshuai Liu,[†] Yi Zhou,[†] Minyong Li,[†] Wenfang Xu,[†] and Hao Fang*[,†]

[†]Department of Medicinal Chemistry, Key Laboratory of Chemical Biology of Natural Products (MOE), School of Pharmacy, Shandong University, Jinan, Shandong 250012, China

[‡]Shandong Cancer Hospital and Institute, Jinan, Shandong 250117, China

Supporting Information

ABSTRACT: As key regulators of epigenetic regulation, human histone deacetylases (HDACs) have been identified as drug targets for the treatment of several cancers. The proper recognition of zinc-binding groups (ZBGs) will help improve the accuracy of virtual screening for novel HDAC inhibitors. Here, we developed a high-specificity ZBG-based pharmacophore model for HDAC8 inhibitors by incorporating customized ZBG features. Subsequently, pharmacophore-based virtual screening led to the discovery of three novel HDAC8 inhibitors with low micromole IC_{50} values (1.8−1.9 μM). Further studies demonstrated that compound **H8-A5** was selective for HDAC8 over HDAC 1/4 and showed antiproliferation activity in MDA-MB-231 cancer cells. Molecular docking and molecular dynamic studies suggested a possible binding mode for **H8-A5**, which provides a good starting point for the development of HDAC8 inhibitors in cancer treatment.

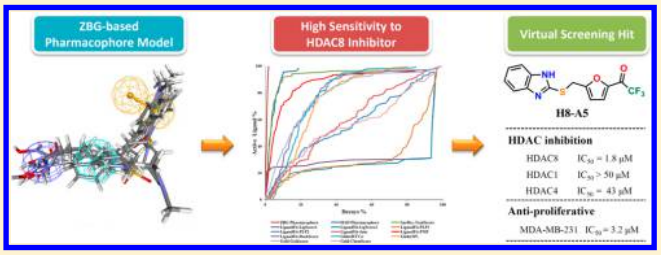

1. INTRODUCTION

The acetylation state of the lysine side chains of histones plays an important role in epigenetic regulation and affects cell cycle progression, transcriptional regulation, and developmental events.[1−3] Lysine acetylation status is regulated by histone deacetylases (HDACs) and histone acetyltransferases (HATs), which catalyze the removal and addition of acetyl groups, respectively.[4−8] Currently, 18 HDAC family members have been identified and categorized as zinc-dependent enzymes (HDAC1-11) and NAD^+-dependent enzymes (SIRT1-7).[9,10] Zinc-dependent HDACs can be further divided into the following four groups: class I (HDACs 1, 2, 3, 8), class IIa (HDACs 4, 5, 7, 9), class IIb (HDACs 6, 10), and class IV (HDAC11).[11−13] Previous studies have shown that HDAC inhibition facilitates gene transcription and ultimately leads to cell differentiation, cell-growth arrest, and apoptosis.[14−16] A large number of HDAC inhibitors have been developed and have shown potential for the treatment of cancer.[14−17] Three HDAC inhibitors (vorinostat, romidepsin, and belinosta) have been approved for the treatment of cutaneous T-cell lymphoma (CTCL) and peripheral T-cell lymphoma (PTCL).[18−20] The structure of most HDAC inhibitors can be divided into the following three parts: a cap group, a hydrophobic linker, and a zinc-binding group (ZBG) (Figure 1).

Over the past two decades, virtual screening has been used in the identification of novel inhibitors of various target proteins.[21−27] There are several approaches to searching commercial databases for novel lead compounds, and these approaches can be subdivided into ligand-based virtual screening (LBVS) and structure-based virtual screening (SBVS).[28−34] The LBVS strategy depends on the information provided by active compounds and can be performed by a variety of methods, including similarity searching,[35,36] pharma-

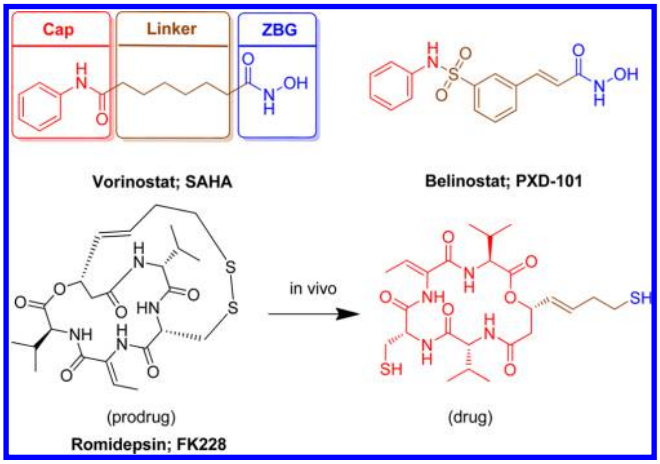

Figure 1. Chemical structure of the three FDA-approved HDAC inhibitors. Romidepsin (FK228) is a prodrug; the disulfide bridge can be reduced by glutathione after cellular uptake.

Received: December 24, 2014
Published: March 10, 2015

DOI: 10.1021/ci500762z
J. Chem. Inf. Model. 2015, 55, 861−871

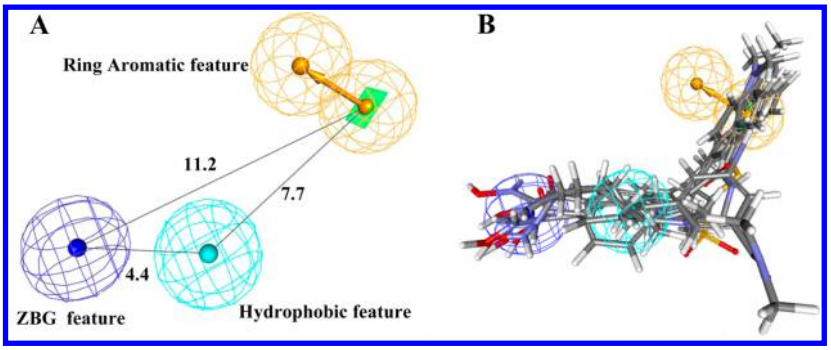

Figure 2. (A) ZBG-based pharmacophore model for HDAC8 inhibitors with distance constraints. (B) Overlay of HDAC8 inhibitors in cocrystal structures in the ZBG-based pharmacophore model.

cophore matching,[29,30] or 3D-QSAR.[37,38] In contrast, SBVS methods are predominantly based on molecular docking.[31]

However, in case of HDAC inhibitors, only a few virtual-screening studies have been reported,[39−42] likely because the current virtual screening methods cannot properly address the zinc-chelating interaction, which is essential for HDAC inhibition. For example, it is difficult for the currently available docking algorithms to predict both the coordination geometry and the interaction strength of HDAC inhibitors with zinc. Although recent studies using specific force field or QM/MM methods[43−45] have shown promising improvements, these strategies are still not suitable for large-scale virtual screening. In the case of the LBVS pharmacophore-matching approach, several pharmacophore models for HDAC inhibitors have already been developed; however, the ZBGs were represented by hydrogen bond donor/acceptor features.[46−48] Thus, the models have a problem with low specificity, particularly in the recognition of ZBGs. For example, the very common chemical amide or sulfamide moieties may be mistakenly recognized as ZBGs in HDAC inhibition studies.

The proper recognition of ZBGs in HDAC inhibitors could be a useful strategy to improve the accuracy of virtual screening. In 2006, Rella et al. successfully employed a customized ZBG pharmacophore feature in the virtual screening of novel angiotensin converting enzyme 2 (ACE2) inhibitors. However, the zinc-chelating fragments identified for ACE2 or other zinc-dependent metalloenzymes, including carbonic anhydrase (hCAII) and matrix metalloproteinases (MMPs), are not directly transferrable to HDACs due to differences in active site charge and geometry.[49,50] Since the discovery of SAHA (vorinostat), the strongly zinc-chelating fragment hydroxamic acid has been widely employed in the design of HDAC inhibitors. Recently, several nonhydroxamate ZBGs have been developed that could further improve the isoform selectivity of HDAC inhibitors.[51−55] Additionally, computational studies have suggested a number of fragments that may possess potential zinc-chelating abilities for HDAC inhibitions.[50,56−58]

The aim of this study was to generate highly specific pharmacophore models to use as filters in the virtual screening of HDAC8 inhibitors. Human HDAC8 was chosen as the virtual screening target primarily because (1) more than 20 human HDAC8 structures cocrystallized with different inhibitors are presently available and could serve as good starting points for the generation of a high-sensitivity pharmacophore model; and (2) inhibition of HDAC8 has attracted a great deal of interest, and discovery of novel HDAC8 inhibitors would be helpful to further expand the therapeutic application range of HDAC family.[59−68] To address zinc-chelating interactions, we developed a customized ZBG-pharmacophore feature for HDACs based on a customized pharmacophore feature strategy as well as known HDAC ZBGs. A high-sensitivity ZBG-based pharmacophore model for HDAC8 was generated by incorporating the customized ZBG feature and was subsequently applied to the virtual screening of HDAC8 inhibitors.

2. RESULTS AND DISCUSSION

2.1. Generation of ZBG-Based Pharmacophore Model.

To properly recognize ZBGs in HDAC inhibitors, we generated a customized ZBG pharmacophore feature using Discovery Studio 2.5. A ZBG library containing 17 known ZBGs and 22 computationally predicted ZBGs (Supporting Information Figure S1) was used to produce the customized ZBG pharmacophore features. Next, the ZBG-based pharmacophore models for HDAC8 inhibitors were constructed by employing the HipHop algorithm. In this process, the bound conformations of six HDAC8 inhibitors extracted from the crystal structures were used. Ten pharmacophore models were produced, and the best one was selected based on the rank values (Supporting Information Table S2). As shown in Figure 2, the ZBG-based pharmacophore model for HDAC8 consists of a ZBG feature, a hydrophobic feature and an aromatic ring feature.

2.2. Evaluation of ZBG-Based Pharmacophore Model.

The discriminatory power of the ZBG-based pharmacophore model was evaluated by screening the HDAC8 subset derived from the DUD-E database,[69] which contains 134 reported HDAC8 inhibitors and more than 10,000 confusing decoys. The confusing decoys were selected from ZINC[70] database by matching the molecular properties with active ligands. As mentioned above, previous studies used hydrogen bond acceptor/donor features to represent ZBGs. Therefore, we also generated a pharmacophore model in which the ZBG was represented by a hydrogen-bond acceptor and hydrogen-bond donor feature (Supporting Information Figure S2, named HAD-based pharmacophore model) to compare the sensitivity with that of ZBG-based pharmacophore model. In addition to pharmacophore approaches, we evaluated several molecular-docking methods, including Surflex, LigandFit, Glide, and Gold.

All of the ligands in the HDAC8 subset of DUD-E database were screened by two pharmacophore models (the ZBG-based pharmacophore and the HAD-based pharmacophore model) and four docking methods within 11 docking score functions (TotalScore in Surflex; LigScore1, LigScore2, PLP1, PLP2, Jain, PMF and DockScore in LigandFit; G-score in Glide; GoldScore and ChemScore in Gold). Enrichment Factor (EF) values were

DOI: 10.1021/ci500762z
J. Chem. Inf. Model. 2015, 55, 861−871

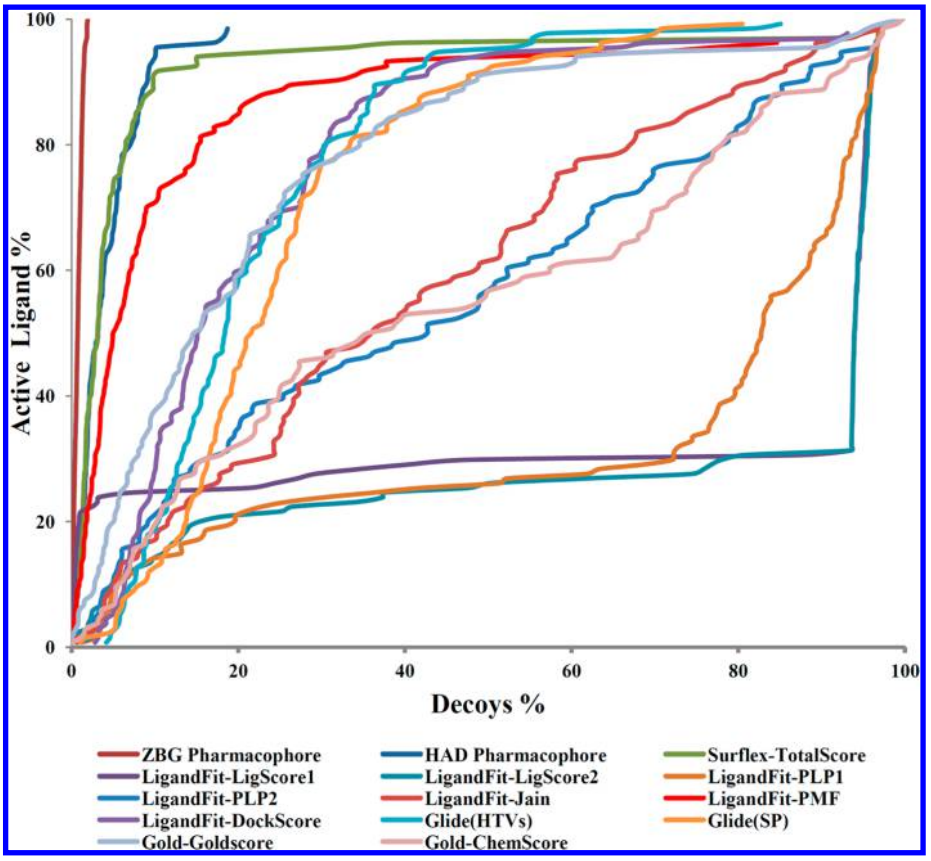

Figure 3. ROC plot of virtual screening method validation.

calculated to measure the discriminatory power of these virtual screening methods.

As shown in Figure 3 and Table 1, the ZBG-based pharmacophore model exhibited significantly better performance compared with the other methods. At 1%, 2%, and 5% of the total database screened, the EF values for ZBG-based pharmacophore model were 67.2, 50, and 20, respectively. It should be mentioned that all known active ligands were found in the top 1% of the screened database when using the ZBG-based pharmacophore model. Although it performed better than most of the docking methods, the HAD-based pharmacophore model was less sensitive than ZBG-based pharmacophore, with EF values of 16.4, 18.3, and 13.3 at 1%, 2%, and 5% of the screened database, respectively. TotalScore of Surflex produced results similar to those of the HAD-based pharmacophore model, which was the best performance among these docking methods.

Table 1. Enrichment Factors for the Different Virtual Screening Methods Validated

screening methods	enrichment factor		
	1%	2%	5%
ZBG pharmacophore	67.2	50.0	20.0
HAD pharmacophore	16.4	18.3	13.3
Surflex Totalscore	14.9	18.9	14.8
LigandFit LigScore1	21.6	11.1	4.9
LigandFit LigScore2	2.2	2.2	2.1
LigandFit PLP1	0.0	0.4	1.8
LigandFit PLP2	0.7	0.4	2.2
LigandFit Jain	1.5	1.1	1.9
LigandFit PMF	11.2	11.1	10.1
LigandFit DockScore	0.0	0.0	1.2
Glide (HTVs)	0.0	0.0	0.4
Glide (SP)	0.0	0.7	0.4
Gold GoldScore	6.2	3.7	3.9
Gold ChemScore	0.8	1.5	1.2

In terms of the seven score functions of LigandFit, LigandScore1, and PMF yielded better results than did LigScore2, PLP1, PLP2, Jain, PMF, and DockScore, which failed to recognize most of the active hits in the top 5% of the screened database. Although the LigScore1 output had the second high EF value at 1% (21.6), the $EF_{5\%}$ was only 4.9, which indicates that it failed to properly rank many of the active ligands. GoldScore only had moderate discriminatory power, but it was better than ChemScore. It is difficult for Glide to rank active ligands properly, and the worst EF value came from either HTVs or the SP mode of Glide. The EF calculations show that the ZBG-based pharmacophore model exhibited the highest specificity and sensitivity to HDAC8 inhibitors compared with the HAD-based pharmacophore model and 11 docking-score functions.

2.3. Virtual Screening Using a ZBG-Based Pharmacophore Model. Virtual screening was performed according to the workflow summarized in Figure 4. First, all ligands in the commercial SPECS database (approximately 200,000 compounds) were prepared using Sybyl-x 1.1. Lipinski's rule of five served as the first filter to obtain a smaller database containing only drug-like compounds (approximately 150,000 compounds). Next, the ZBG-based pharmacophore model was used to screen these drug-like compounds, and 358 compounds

DOI: 10.1021/ci500762z
J. Chem. Inf. Model. 2015, 55, 861−871

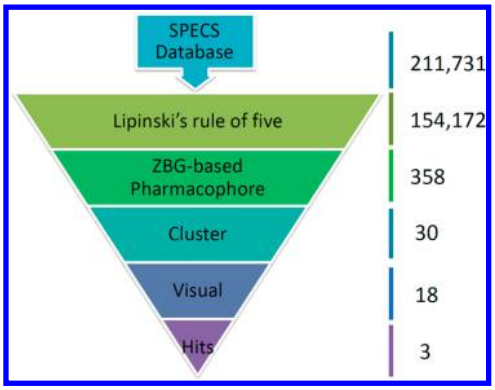

Figure 4. Protocol for ZBG pharmacophore-based virtual screening.

that could map the ZBG feature were selected. Cluster analysis divided the 358 compounds into 10 groups by structural features. Compounds in every group were arranged based on fit values; the three top-ranked compounds from each cluster group were selected, leading to total of 30 candidate compounds. In the next step, visual selection was performed, mainly considering the structural diversity of potential zinc binding groups; 18 commercially available compounds were finally selected and purchased.

2.4. Enzyme Inhibition and Predicted Binding Mode. All of the virtual screening hits were purchased from the SPECS database with purities >95% (confirmed by SPECS, Figure 5). HDAC8 inhibitory potencies were preliminarily tested at a concentration of 50 μM, and only compounds that exhibited more than 50% inhibition were further tested at different concentrations to calculate IC_{50} values (Table 2). Finally, three compounds (**H8-A3**, **H8-A4**, and **H8-A5**) were identified as novel HDAC8 inhibitors with IC_{50} values (1.8 μM, 1.8 μM, and 1.9 μM, respectively) comparable to the IC_{50} of SAHA (4.3 μM) (Table 3). The dose-dependent plot of the inhibitors **H8-A3**, **H8-A4**, and **H8-A5** is shown in Supporting Information Figure S3, Figure S4, and Figure S5.

To further explore the structural basis of HDAC8 inhibition of the identified inhibitors, we docked **H8-A3**, **H8-A4**, and **H8-A5** into the active site of HDAC8 (PDB ID: 1T64). To validate the docking protocols, we docked the ligands extracted from cocrystal structures of HDAC8 back to the corresponding proteins. Initially, molecular dockings were performed using AutoDock 4.2 and Surflex, but the former often failed to reproduce the chelation interactions between ligands and the zinc ion. In a redocking study using Surflex, the ZBGs were located near the zinc at the bottom of the HDAC8 binding pocket (Zn−O distance approximately 2.0 Å), and the binding pose of most ligands in the crystal structures could be reproduced with RMSD values ranging from 1.4 to 3.3 Å (Supporting Information Table S3). Thus, **H8-A3**, **H8-A4**, and **H8-A5** were docked into HDAC8 using Surflex, and the top-

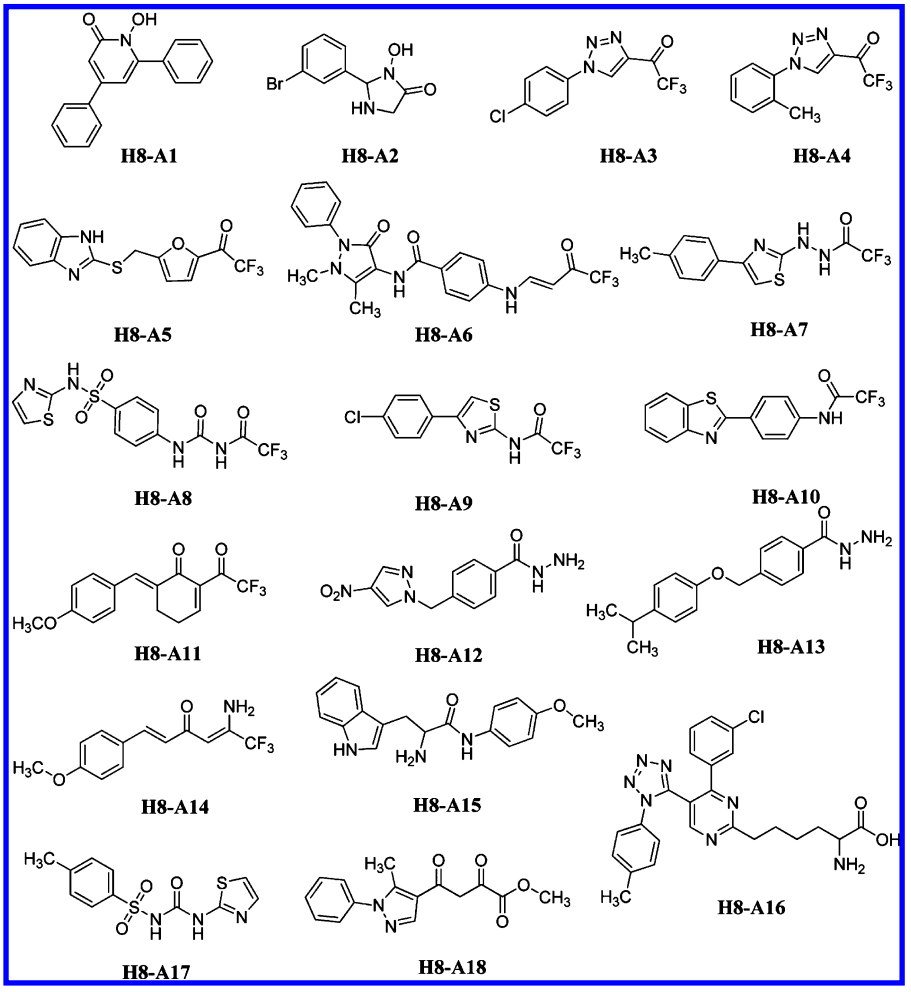

Figure 5. Chemical structure of selected virtual screening hits.

DOI: 10.1021/ci500762z
J. Chem. Inf. Model. 2015, 55, 861−871

Table 2. Mapped Pharmacophore Features of the Selected Compounds and Their HDAC8 Inhibition

compound	mapped features	% inhibition of HDAC8 at 50 μM
H8-A1	ZBG, HY	2
H8-A2	ZBG, HY	9
H8-A3	ZBG, HY	**76**
H8-A4	ZBG, HY	**79**
H8-A5	ZBG, HY, AR	**80**
H8-A6	ZBG, HY, AR	14
H8-A7	ZBG, HY	17
H8-A8	ZBG, HY, AR	8
H8-A9	ZBG, HY	20
H8-A10	ZBG, HY	37
H8-A11	ZBG, HY	22
H8-A12	ZBG, HY	15
H8-A13	ZBG, HY, AR	4
H8-A14	ZBG, HY	22
H8-A15	ZBG, HY	4
H8-A16	ZBG, HY, AR	2
H8-A17	ZBG, HY	7
H8-A18	ZBG, HY	4

scored conformations for each compound were chosen to present the possible binding mode.

As shown in Figure 6, the trifluoroacetyl groups of **H8-A3**, **H8-A4**, and **H8-A5** could interact with the zinc atom with distances between the zinc atom and the oxygen atom in the carbonyl group (Zn−O) < 2 Å. Hydrogen-bond interactions with Y306 could be found for **H8-A3**, **H8-A4**, and **H8-A5**. Moreover, **H8-A5** could form another hydrogen bond with D101. Additionally, a hydrophobic interaction between F152 and F208 was predicted in these three inhibitors.

2.5. HDAC Isoform Selectivity and in Vitro Anti-proliferative Assay. Although the exact mechanism by which HDACs selectively regulate specific genes is poorly understood, it is obvious that the selective inhibition of specific HDACs over others is highly desirable and more likely to yield specific and nontoxic drugs. The undesirable side effects of the pan inhibitor, SAHA (e.g., bone marrow depression, diarrhea, weight loss, and cardiac arrhythmias),[71] have made further clinical development difficult. Isoform-selective HDAC inhibitors will be helpful to develop more effective inhibitors with fewer side effects.[72,73]

Therefore, we evaluated the selectivity of the newly identified inhibitors, **H8-A3**, **H8-A4**, and **H8-A5**, against HDAC1 and HDAC4. These inhibitors exhibited more than 16-fold greater selectivity for HDAC8 over HDAC1. In terms of HDAC4 inhibition, **H8-A3** and **H8-A4** had similar IC_{50} values (1.4 μM and 0.67 μM, respectively) compared with their HDAC8 inhibition. It should be noted that the previously reported trifluoromethyl ketone-based HDAC inhibitors also exhibit strong inhibition of HDAC4. Importantly, **H8-A5** exhibited more than 20-fold increased selectivity for HDAC8 over HDAC4.

Next, we sought to examine the antiproliferative activities of these compounds. Three tumor cell lines, MDA-MB231, HCT116, and A549 were tested using an SRB assay. As shown in Table 3, **H8-A5** exhibited better antiproliferative activity in the MDA-MB-231 cell line (IC_{50} = 3.6 μM) compared with that in HCT116 (IC_{50} = 76 μM). However, **H8-A3** showed weak antiproliferative activity (IC_{50} = 30.9 μM in MDA-MB-231 cell line; 61 μM in HCT116 cell line), and **H8-A4** was inactive in these cancer cell lines (IC_{50} > 100 μM). No compound showed good inhibitory activities against A549 cell line. The inhibition curves of inhibitors **H8-A3** and **H8-A5** against MDA-MB-231 and HCT116 cell lines are shown in Supporting Information Figure S6 and Figure S7.

2.6. Insight into the Binding of H8-A5 to HDAC8. In vitro tests have confirmed that **H8-A5** is a HDAC8-selective inhibitor with antiproliferative activities. To obtain structural insights into the inhibition mechanism of **H8-A5**, the HDAC8:**H8-A5** complex predicted by molecular docking (Figure 6C) was subjected to 50 ns molecular dynamics simulation. The overall binding stability, the retention of ligand hydrogen-bond contacts, and deviations in the protein structure were analyzed.

To validate the stability of the binding complex, the root-mean square deviation (RMSD) of the complex was calculated. The conformation of the HDAC8:**H8-A5** complex stabilized after approximately 1 ns of simulation, and the average RMSD values were below 0.15 nm (Figure 7A). **H8-A5** remained in the binding pocket during the simulation, with the potential zinc-binding trifluoroacetyl moieties located near the catalytic divalent Zn^{2+} ion (Video S1). The distance between the trifluoroacetyl moieties and the Zn^{2+} ion (Zn−O) was measured throughout the simulations. The average Zn−O distance was stably maintained at 0.19 nm. We also detected hydrogen-bond interactions between **H8-A5** and residues D101/Y306, which were predicted by docking. As shown in Figures 6C and 6D, a hydrogen-bond interaction between **H8-A5** and D101 was observed during the simulation, whereas the interaction between **H8-A5** and Y306 was dismissed.

Root-mean square fluctuation (RMSF) plots were made to determine the flexibility of residues in the binding pocket during the simulation. Most of the catalytically important residues were stable, whereas the surface hydrophobic residues such as Y100, F152, and Y306 showed a certain degree of flexibility (Figure 8 and Video S2). We performed a cluster analysis using *g_cluster*, and six representative conformations for these three residues were selected (Figure 8B). These results suggested that the binding pocket of HDAC8 is malleable, allowing interaction with different inhibitors. It should be noted that crystal structures of HDAC8 complexed with inhibitors show different conformations of the HDAC8

Table 3. In Vitro Inhibitory Activities against HDAC Isoforms and Anti-Proliferative Activities

	HDAC inhibition IC_{50} (μM)			antiproliferative IC_{50} (μM)		
compound	HDAC8	HDAC1	HDAC4	MDA-MB-231	HCT116	A549
H8-A3	1.9	31	1.4	30.9	61	>100
H8-A4	1.8	>50	0.67	>100	>100	>100
H8-A5	1.8	>50	43	3.6	76	>100
SAHA	4.3	0.061	>50	0.21	0.49	0.49

DOI: 10.1021/ci500762z
J. Chem. Inf. Model. 2015, 55, 861−871

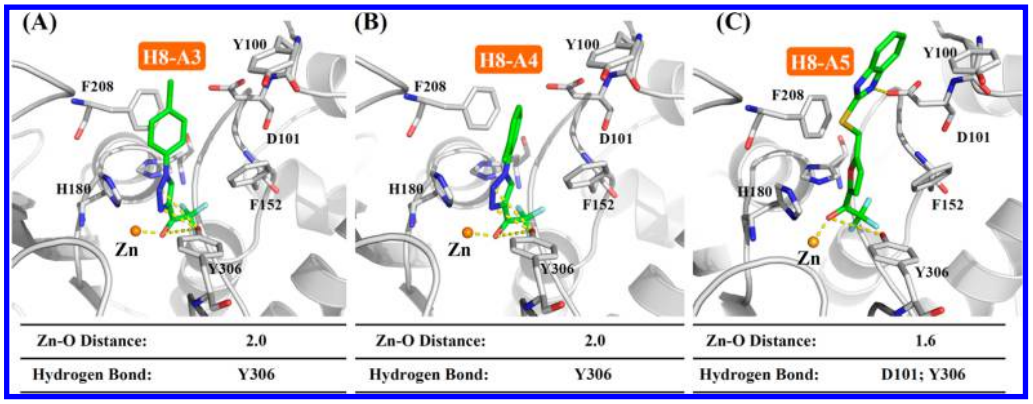

Figure 6. Proposed binding mode of compound **H8-A3** (A), **H8-A4** (B), and **H8-A5** (C). The distance between the zinc ion and oxygen atom (trifluoroacetyl group) and the residues that could form a hydrogen bond with the inhibitor were listed.

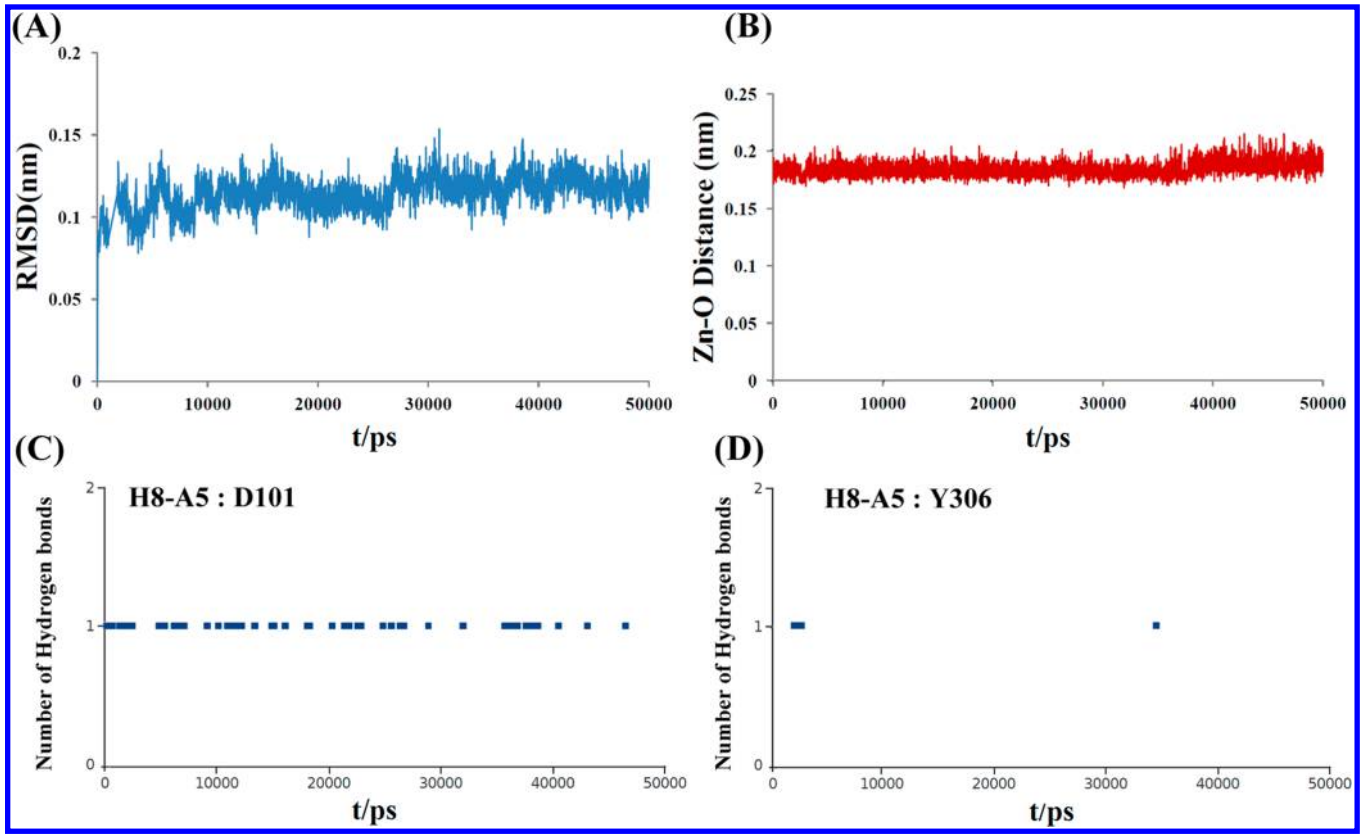

Figure 7. (A) Backbone RMSD values during molecular dynamic simulation; (B) Zn−O distances during molecular dynamic simulation; (C) Number of hydrogen bonds between **H8-A5** and D101 during molecular dynamic simulation; (D) Number of hydrogen bonds between **H8-A5** and Y306 during molecular dynamic simulation.

surface.[59,65,74−76] In general, these computational results were beneficial for the future design of HDAC8-selective inhibitors.

3. CONCLUSIONS

In the present work, we describe the generation and application of a ZBG-based pharmacophore model for HDAC8 inhibitors. The sensitivity of the pharmacophore model was significantly improved by incorporating customized ZBG features. In the investigation using the DUD database, most of the confusing decoys could not match the ZBG-based pharmacophore model due to the lack of potential ZBGs. Considering the critical roles of zinc chelating interactions in the binding of HDAC8 inhibitors, the high specific ZBG-based pharmacophore model could serve as an efficient virtual screening strategy for HDAC8 inhibitors. Then, pharmacophore-based virtual screening of the SPECS database led to the discovery of three novel trifluoroacetyl-based HDAC8 inhibitors with low micromolar activity (1.8−1.9 μM). Further in vitro tests demonstrated that compound **H8-A5** possessed a certain degree of selectivity for HDAC8 over HDAC1/4 and showed good antiproliferative activity in the MDA-MB-231 cancer cell line. The subsequent 50 ns molecular dynamic simulation of HDAC8:**H8-A5** complex suggested a chelating interaction between the trifluoroacetyl group and the zinc ion as well as a hydrogen-bond interaction between **H8-A5** and D101. The flexibility of three residues in the HDAC8 active site (Y100, F152, and Y306) was also observed.

DOI: 10.1021/ci500762z
J. Chem. Inf. Model. 2015, 55, 861−871

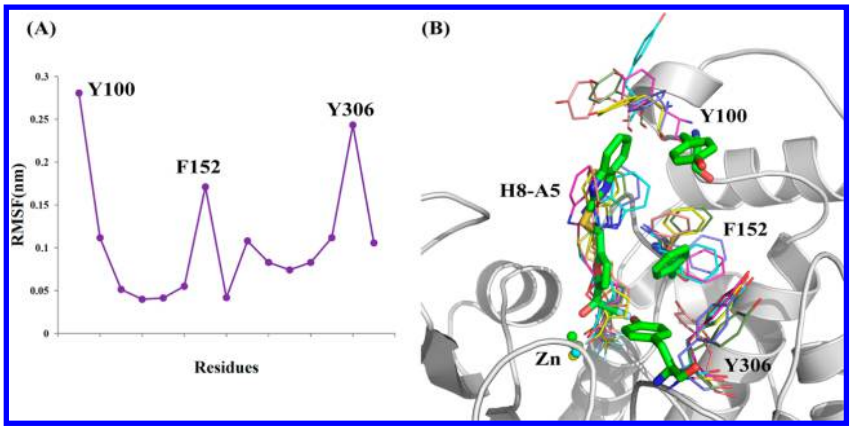

Figure 8. (A) RMSF values of residues in the HDAC8 active site during the molecular dynamic simulation. (B) Overlay of the initial conformation of the HDAC8:**H8-A5** complex (inhibitor and residues Y100, F152, and Y306 are presented as green stick) and the six representative conformations during a 50 ns simulation (inhibitors and flexible residues are presented in line with different colors).

Taken together, these newly identified trifluoroacetyl-based HDAC8 inhibitors confirmed the successful application of a customized ZBG feature in pharmacophore-based virtual screening for HDAC inhibitors. Furthermore, the most potent and selective inhibitor **H8-A5** could serve as a useful lead compound in the design of HDAC8-selective inhibitors for the treatment of cancer.

4. MATERIALS AND METHODS

4.1. Pharmacophore Model Generation and Validation. To date, more than 20 crystal structures of human HDAC8 cocrystallized with different inhibitors have been determined. Where different crystal structures contained the same inhibitor, priority was given to the structure with higher resolution. The crystal structures of HDAC8 mutants were not used. Additionally, 2V5X was not used because the molecular weight of the inhibitor was 624.42 Da, which violates Lipinski's rule of five for drug-like compounds. Finally, six HDAC8 inhibitors extracted from cocrystal structures (PDB IDs: 1T64, 1T67, 1T69, 1W22, 3F07, and 1VKG) were used to generate a pharmacophore model in Accelrys Discovery Studio 2.5. During the process of generating pharmacophore models, five chemical features were selected, including ZBG, hydrogen-bond acceptor, hydrogen-bond donor, hydrophobic, and aromatic ring. Because the ZBG feature was not provided in the feature dictionary of Discovery Studio 2.5, we generated a customized ZBG feature by replacing the negative ionizable (NI) feature using the *Customize Pharmacophore Features* in Discovery Studio 2.5 tools. The customized ZBG feature was modified to detect a ZBG library (Supporting Information, Figure S1) which contains 17 ZBGs from known HDAC inhibitors and 22 predicted ZBGs selected from a computational study.[50]

No prior diverse conformation-generation step was performed because the crystal-bound conformations of the inhibitors should represent bioactive conformations. Other control parameters were set at the default values. Ten pharmacophore models were generated, and the best one was selected as the ZBG-based pharmacophore model based on the rank values.

Pharmacophore sensitivity validation was performed by screening a test set database of 134 compounds with HDAC8 inhibition activity and another 10450 structurally diverse compounds within the HDAC8 subset of the DUD-E database. We also constructed a HAD-based pharmacophore model in which the zinc-binding group was represented by a hydrogen-bond acceptor and a hydrogen-bond donor feature using a method similar to the construction of the ZBG-based pharmacophore model. Additionally, molecular docking methods including Surflex, LigandFit, Glide, and Gold were validated. The docking parameters and calculation of enrichment factor (EF) have been previously described.[25]

4.2. Database Preparation and Virtual Screening. The SPECS database, which contains more than 200,000 small molecule compounds, was filtered with Lipinski's rule of five (molecular weight $\leq$ 500, SlogP $\leq$ 5, number of hydrogen bond donors $\leq$ 5, number of hydrogen bond acceptors $\leq$ 10, number of rotatable bonds $\leq$ 10) to construct a theoretical drug-like SPECS database. The ZBG-based pharmacophore model was used to screen the theoretical drug-like SPECS database with a flexible search method within Discovery Studio 2.5. During this process, the CAESAR conformation generation method was used with the maximum number of conformers generated set to 255. Cluster analysis was performed based on the FCFP_6 fingerprints calculation. The other parameters were set to the default values. The selected compounds were purchased from SPECS, and the purities were confirmed using LC-MS and ^{1}H NMR.

4.3. In Vitro HDAC Inhibition Assays. The HDAC8 and HDAC4 enzyme were purchased from SignalChem (#H90-30H, #H86-31G). The HDAC1 enzyme was purchased from Abcam (#AB101661). In vitro activity against HDAC was determined as previously described.[77] Briefly, HDAC enzymes were mixed with various concentrations of compound sample (diluted in DMSO). After addition of substrate, the mixture was incubated at 37 °C for 30 min and then stopped by addition of trypsin and TSA. Fluorescence is then analyzed using SpectraMax M5 microtiter plate reader with an excitation wavelength of 350−360 nm and an emission wavelength of 450−460 nm. The IC_{50} values were calculated using GraphPad Prism.

4.4. Cell Culture and Cell Proliferation Assay. All cell lines were maintained in RPMI 1640 medium containing 10% FBS at 37 °C in a 5% CO_2 humidified incubator. Cell proliferation was determined by the SRB (sulforhodamine B) method. Briefly, cells were passaged the day before dosing into a 96-well cell plate, allowed to grow for a minimum of 24 h, and then treated with different concentrations of test compounds for 72 h. The cells were fixed with 10% TCA and stained with

DOI: 10.1021/ci500762z
J. Chem. Inf. Model. 2015, 55, 861−871

SRB. The excess dye was washed away, and the remaining bound SRB dye was extracted from the cells with Tris base buffer. Absorbance was measured using a SPECTRAmax 190 reader at 565 nm. The data were analyzed using GraphPad Prism to calculate the IC_{50}.

4.5. Binding Mode Prediction. Binding modes were predicted by molecular docking with Surflex[78,79] and Autodock 4.2.[31] The crystal structure of HDAC8-TSA (PDB ID: 1T64) was used. Protein structures were prepared with Sybyl-x 1.1 (Tripos, Inc.) by adding hydrogen atoms, protonating the ionizable residues at neutral pH, and calculating AMBER FF99 charges for the protein. Default values for the critical parameters were chosen, and the details for each program are shown below.

Surflex. The active site was generated based on the ligand in the crystal structure. Favorable target-ligand interactions were detected using probe atoms, and ligand fragments were aligned to the best interaction points. TotalScore was used to sort the docked conformations, and the top-scored results were chosen to represent the possible binding mode.

Autodock. One hundred docking calculations were performed employing the Lamarckian Genetic Algorithm (LGA) with default parameters. A grid size of 60 × 60 × 60 points with a grid spacing of 0.375 Å was applied, and the grid box was centered on the original ligand in cocrystal structure. All docked conformations were clustered based on the root-mean-square deviation (RMSD) values. Top-scored conformations in first cluster were selected as the best docking result.

4.6. Molecular Dynamic. Molecular dynamic simulations were performed using GROMACS 4.5.2[80,81] and the AMBER99SB-ILDN force field.[82] Side-chains in HDAC8 (PDB ID: 1T64) were repaired using Sybyl-x 1.1 and verified using Modeler 9.[83] The system was solvated in a cubic box of TIP3P water molecules and neutralized with counterions, and energy minimization was performed using steepest descent for 5000 steps. Then a 50 ps position restrained molecular dynamics run was performed, during which the protein backbone was frozen, and solvent molecules as well as counterions were allowed to move. Finally, 50 ns of production run was performed in an NPT ensemble using an isotropic Parrinello−Rahman pressure coupling, Nosé-Hover thermostat at 300 K, and periodic boundary conditions. The van der Waals interactions and short-range electrostatic employed a cutoff of 1.0 nm. Long-range electrostatics interactions were treated using the Particle Mesh Ewald (PME) method.[84] The P-LINCS algorithm was applied to fix all bonds containing hydrogen atoms.[85] The coordinates were stored every 2 ps, and the simulation time step was 2 fs. The topology file for compound **H8-A5** was generated using PRODRG.[86] The protonation states of histidines were calculated using the H++ server,[87] and the protonation states of histidines 142 and 143, which are close to the catalytic site, were protonated on the δ nitrogen as described in the literature.[67] The trajectory was analyzed using GROMACS package, VMD 1.9, and PyMOL 1.4.1.

■ ASSOCIATED CONTENT

Supporting Information

Additional information as noted in the text. This material is available free of charge via the Internet at http://pubs.acs.org.

■ AUTHOR INFORMATION

Corresponding Author

*Phone: 86-531-88382731. Fax: 86-531-88382548. E-mail: haofangcn@sdu.edu.cn.

Notes

The authors declare no competing financial interest.

■ ACKNOWLEDGMENTS

We are very grateful to Professor Renxiao Wang at the Shanghai Institute of Organic Chemistry, Chinese Academy of Sciences, for providing the necessary software. This work was supported by the National Natural Science Foundation of China (Grant 81373281), the Shandong Natural Science Fund for Distinguished Young Scholars (Grant JQ201319), the Program for New Century Excellent Talents in University (Grant NCET-12-0337), and the Program for Changjiang Scholars and Innovative Research Team in University, PCSIRT (Grant IRT13028).

■ REFERENCES

(1) Rodriguez-Paredes, M.; Esteller, M. Cancer epigenetics reaches mainstream oncology. *Nat. Med.* **2011**, *17*, 330−9.

(2) Arrowsmith, C. H.; Bountra, C.; Fish, P. V.; Lee, K.; Schapira, M. Epigenetic protein families: a new frontier for drug discovery. *Nat. Rev. Drug Discovery* **2012**, *11*, 384−400.

(3) Grunstein, M. Histone acetylation in chromatin structure and transcription. *Nature* **1997**, *389*, 349−52.

(4) Choudhary, C.; Kumar, C.; Gnad, F.; Nielsen, M. L.; Rehman, M.; Walther, T. C.; Olsen, J. V.; Mann, M. Lysine acetylation targets protein complexes and co-regulates major cellular functions. *Science* **2009**, *325*, 834−40.

(5) Glozak, M. A.; Sengupta, N.; Zhang, X.; Seto, E. Acetylation and deacetylation of non-histone proteins. *Gene* **2005**, *363*, 15−23.

(6) Gui, C. Y.; Ngo, L.; Xu, W. S.; Richon, V. M.; Marks, P. A. Histone deacetylase (HDAC) inhibitor activation of p21WAF1 involves changes in promoter-associated proteins, including HDAC1. *Proc. Natl. Acad. Sci. U. S. A.* **2004**, *101*, 1241−6.

(7) Zhao, S.; Xu, W.; Jiang, W.; Yu, W.; Lin, Y.; Zhang, T.; Yao, J.; Zhou, L.; Zeng, Y.; Li, H.; Li, Y.; Shi, J.; An, W.; Hancock, S. M.; He, F.; Qin, L.; Chin, J.; Yang, P.; Chen, X.; Lei, Q.; Xiong, Y.; Guan, K. L. Regulation of cellular metabolism by protein lysine acetylation. *Science* **2010**, *327*, 1000−4.

(8) Yang, X. J.; Seto, E. HATs and HDACs: from structure, function and regulation to novel strategies for therapy and prevention. *Oncogene* **2007**, *26*, 5310−8.

(9) Bieliauskas, A. V.; Pflum, M. K. Isoform-selective histone deacetylase inhibitors. *Chem. Soc. Rev.* **2008**, *37*, 1402−13.

(10) Marson, C. M.; Matthews, C. J.; Yiannaki, E.; Atkinson, S. J.; Soden, P. E.; Shukla, L.; Lamadema, N.; Thomas, N. S. Discovery of potent, isoform-selective inhibitors of histone deacetylase containing chiral heterocyclic capping groups and a N-(2-aminophenyl)-benzamide binding unit. *J. Med. Chem.* **2013**, *56*, 6156−74.

(11) Wang, D. F.; Helquist, P.; Wiech, N. L.; Wiest, O. Toward selective histone deacetylase inhibitor design: homology modeling, docking studies, and molecular dynamics simulations of human class I histone deacetylases. *J. Med. Chem.* **2005**, *48*, 6936−47.

(12) Ortore, G.; Di Colo, F.; Martinelli, A. Docking of hydroxamic acids into HDAC1 and HDAC8: a rationalization of activity trends and selectivities. *J. Chem. Inf. Model.* **2009**, *49*, 2774−85.

(13) Wambua, M. K.; Nalawansha, D. A.; Negmeldin, A. T.; Pflum, M. K. Mutagenesis studies of the 14 A internal cavity of histone deacetylase 1: insights toward the acetate-escape hypothesis and selective inhibitor design. *J. Med. Chem.* **2014**, *57*, 642−50.

(14) Lane, A. A.; Chabner, B. A. Histone deacetylase inhibitors in cancer therapy. *J. Clin. Oncol.* **2009**, *27*, 5459−68.

DOI: 10.1021/ci500762z
J. Chem. Inf. Model. 2015, 55, 861−871

(15) Garber, K. HDAC inhibitors overcome first hurdle. *Nat. Biotechnol.* **2007**, *25*, 17−9.
(16) Zhang, L.; Han, Y.; Jiang, Q.; Wang, C.; Chen, X.; Li, X.; Xu, F.; Jiang, Y.; Wang, Q.; Xu, W. Trend of Histone Deacetylase Inhibitors in Cancer Therapy: Isoform Selectivity or Multitargeted Strategy. *Med. Res. Rev.* **2015**, *35*, 63−84.
(17) Paris, M.; Porcelloni, M.; Binaschi, M.; Fattori, D. Histone deacetylase inhibitors: from bench to clinic. *J. Med. Chem.* **2008**, *51*, 1505−29.
(18) Glaser, K. B. HDAC inhibitors: clinical update and mechanism-based potential. *Biochem. Pharmacol.* **2007**, *74*, 659−71.
(19) Kirschbaum, M. H.; Foon, K. A.; Frankel, P.; Ruel, C.; Pulone, B.; Tuscano, J. M.; Newman, E. M. A phase 2 study of belinostat (PXD101) in patients with relapsed or refractory acute myeloid leukemia or patients over the age of 60 with newly diagnosed acute myeloid leukemia: a California Cancer Consortium Study. *Leuk. Lymphoma* **2014**, *55*, 2301−4.
(20) Wagner, J. M.; Hackanson, B.; Lubbert, M.; Jung, M. Histone deacetylase (HDAC) inhibitors in recent clinical trials for cancer therapy. *Clin. Epigenet.* **2010**, *1*, 117−136.
(21) Lavecchia, A.; Di Giovanni, C.; Cerchia, C.; Russo, A.; Russo, G.; Novellino, E. Discovery of a novel small molecule inhibitor targeting the frataxin/ubiquitin interaction via structure-based virtual screening and bioassays. *J. Med. Chem.* **2013**, *56*, 2861−73.
(22) Alcaro, S.; Musetti, C.; Distinto, S.; Casatti, M.; Zagotto, G.; Artese, A.; Parrotta, L.; Moraca, F.; Costa, G.; Ortuso, F.; Maccioni, E.; Sissi, C. Identification and characterization of new DNA G-quadruplex binders selected by a combination of ligand and structure-based virtual screening approaches. *J. Med. Chem.* **2013**, *56*, 843−55.
(23) Osolodkin, D. I.; Kozlovskaya, L. I.; Dueva, E. V.; Dotsenko, V. V.; Rogova, Y. V.; Frolov, K. A.; Krivokolysko, S. G.; Romanova, E. G.; Morozov, A. S.; Karganova, G. G.; Palyulin, V. A.; Pentkovski, V. M.; Zefirov, N. S. Inhibitors of tick-borne flavivirus reproduction from structure-based virtual screening. *ACS Med. Chem. Lett.* **2013**, *4*, 869−74.
(24) Bowers, E. M.; Yan, G.; Mukherjee, C.; Orry, A.; Wang, L.; Holbert, M. A.; Crump, N. T.; Hazzalin, C. A.; Liszczak, G.; Yuan, H.; Larocca, C.; Saldanha, S. A.; Abagyan, R.; Sun, Y.; Meyers, D. J.; Marmorstein, R.; Mahadevan, L. C.; Alani, R. M.; Cole, P. A. Virtual ligand screening of the p300/CBP histone acetyltransferase: identification of a selective small molecule inhibitor. *Chem. Biol.* **2010**, *17*, 471−82.
(25) Hou, X.; Li, R.; Li, K.; Yu, X.; Sun, J. P.; Fang, H. Fast identification of novel lymphoid tyrosine phosphatase inhibitors using target-ligand interaction-based virtual screening. *J. Med. Chem.* **2014**, *57*, 9309−22.
(26) Xu, L.; Zhang, Y.; Zheng, L.; Qiao, C.; Li, Y.; Li, D.; Zhen, X.; Hou, T. Discovery of novel inhibitors targeting the macrophage migration inhibitory factor via structure-based virtual screening and bioassays. *J. Med. Chem.* **2014**, *57*, 3737−45.
(27) Siddiquee, K.; Zhang, S.; Guida, W. C.; Blaskovich, M. A.; Greedy, B.; Lawrence, H. R.; Yip, M. L.; Jove, R.; McLaughlin, M. M.; Lawrence, N. J.; Sebti, S. M.; Turkson, J. Selective chemical probe inhibitor of Stat3, identified through structure-based virtual screening, induces antitumor activity. *Proc. Natl. Acad. Sci. U. S. A.* **2007**, *104*, 7391−6.
(28) Ripphausen, P.; Nisius, B.; Peltason, L.; Bajorath, J. Quo vadis, virtual screening? A comprehensive survey of prospective applications. *J. Med. Chem.* **2010**, *53*, 8461−7.
(29) Yang, S. Y. Pharmacophore modeling and applications in drug discovery: challenges and recent advances. *Drug Discovery Today* **2010**, *15*, 444−50.
(30) Leach, A. R.; Gillet, V. J.; Lewis, R. A.; Taylor, R. Three-dimensional pharmacophore methods in drug discovery. *J. Med. Chem.* **2010**, *53*, 539−58.
(31) Hou, X. B.; Du, J. T.; Zhang, J.; Du, L. P.; Fang, H.; Li, M. Y. How to Improve Docking Accuracy of AutoDock4.2: A Case Study Using Different Electrostatic Potentials. *J. Chem. Inf. Model.* **2013**, *53*, 188−200.
(32) Zhang, X.; Li, X.; Wang, R. Interpretation of the binding affinities of PTP1B inhibitors with the MM-GB/SA method and the X-score scoring function. *J. Chem. Inf. Model.* **2009**, *49*, 1033−48.
(33) Li, G. B.; Yang, L. L.; Wang, W. J.; Li, L. L.; Yang, S. Y. ID-Score: a new empirical scoring function based on a comprehensive set of descriptors related to protein-ligand interactions. *J. Chem. Inf. Model.* **2013**, *53*, 592−600.
(34) Tian, S.; Sun, H.; Pan, P.; Li, D.; Zhen, X.; Li, Y.; Hou, T. Assessing an ensemble docking-based virtual screening strategy for kinase targets by considering protein flexibility. *J. Chem. Inf. Model.* **2014**, *54*, 2664−79.
(35) Hahnke, V.; Todoroff, N.; Rodrigues, T.; Schneider, G. Significance estimation for sequence-based chemical similarity searching (PhAST) and application to AuroraA kinase inhibitors. *Future Med. Chem.* **2012**, *4*, 1897−906.
(36) Moffat, K.; Gillet, V. J.; Whittle, M.; Bravi, G.; Leach, A. R. A comparison of field-based similarity searching methods: CatShape, FBSS, and ROCS. *J. Chem. Inf. Model.* **2008**, *48*, 719−29.
(37) Therese, P. J.; Manvar, D.; Kondepudi, S.; Battu, M. B.; Sriram, D.; Basu, A.; Yogeeswari, P.; Kaushik-Basu, N. Multiple e-pharmacophore modeling, 3D-QSAR, and high-throughput virtual screening of hepatitis C virus NS5B polymerase inhibitors. *J. Chem. Inf. Model.* **2014**, *54*, 539−52.
(38) Hou, X.; Du, J.; Fang, H.; Li, M. 3D-QSAR study on a series of Bcl-2 protein inhibitors using comparative molecular field analysis. *Protein Pept. Lett.* **2011**, *18*, 440−9.
(39) Tang, H.; Wang, X. S.; Huang, X. P.; Roth, B. L.; Butler, K. V.; Kozikowski, A. P.; Jung, M.; Tropsha, A. Novel inhibitors of human histone deacetylase (HDAC) identified by QSAR modeling of known inhibitors, virtual screening, and experimental validation. *J. Chem. Inf. Model.* **2009**, *49*, 461−76.
(40) Park, H.; Kim, S.; Kim, Y. E.; Lim, S. J. A structure-based virtual screening approach toward the discovery of histone deacetylase inhibitors: identification of promising zinc-chelating groups. *ChemMedChem* **2010**, *5*, 591−7.
(41) Li, G. B.; Yang, L. L.; Yuan, Y.; Zou, J.; Cao, Y.; Yang, S. Y.; Xiang, R.; Xiang, M. Virtual screening in small molecule discovery for epigenetic targets. *Methods* **2015**, *71*, 158−66.
(42) Kandakatla, N.; Ramakrishnan, G. Ligand Based Pharmacophore Modeling and Virtual Screening Studies to Design Novel HDAC2 Inhibitors. *Adv. Bioinf.* **2014**, *2014*, 812148.
(43) Santos-Martins, D.; Forli, S.; Ramos, M. J.; Olson, A. J. AutoDock4(Zn): an improved AutoDock force field for small-molecule docking to zinc metalloproteins. *J. Chem. Inf. Model.* **2014**, *54*, 2371−9.
(44) Pottel, J.; Therrien, E.; Gleason, J. L.; Moitessier, N. Docking Ligands into Flexible and Solvated Macromolecules. 6. Development and Application to the Docking of HDACs and other Zinc Metalloenzymes Inhibitors. *J. Chem. Inf. Model.* **2014**, *54*, 254−265.
(45) Chaskar, P.; Zoete, V.; Rohrig, U. F. Toward On-The-Fly Quantum Mechanical/Molecular Mechanical (QM/MM) Docking: Development and Benchmark of a Scoring Function. *J. Chem. Inf. Model.* **2014**, *54*, 3137−52.
(46) Thangapandian, S.; John, S.; Sakkiah, S.; Lee, K. W. Ligand and structure based pharmacophore modeling to facilitate novel histone deacetylase 8 inhibitor design. *Eur. J. Med. Chem.* **2010**, *45*, 4409−17.
(47) Chen, Y. D.; Jiang, Y. J.; Zhou, J. W.; Yu, Q. S.; You, Q. D. Identification of ligand features essential for HDACs inhibitors by pharmacophore modeling. *J. Mol. Graphics Modell.* **2008**, *26*, 1160−1168.
(48) Chen, Y. D.; Li, F. F.; Tang, W. Q.; Zhu, C. C.; Jiang, Y. J.; Zou, J. W.; Yu, Q. S.; You, Q. D. 3D-QSAR studies of HDACs inhibitors using pharmacophore-based alignment. *Eur. J. Med. Chem.* **2009**, *44*, 2868−2876.
(49) Day, J. A.; Cohen, S. M. Investigating the selectivity of metalloenzyme inhibitors. *J. Med. Chem.* **2013**, *56*, 7997−8007.
(50) Chen, K.; Xu, L.; Wiest, O. Computational exploration of zinc binding groups for HDAC inhibition. *J. Org. Chem.* **2013**, *78*, 5051−5.

DOI: 10.1021/ci500762z
J. Chem. Inf. Model. 2015, 55, 861−871

(51) Scarpelli, R.; Di Marco, A.; Ferrigno, F.; Laufer, R.; Marcucci, I.; Muraglia, E.; Ontoria, J. M.; Rowley, M.; Serafini, S.; Steinkuhler, C.; Jones, P. Studies of the metabolic stability in cells of 5-(trifluoroacetyl)thiophene-2-carboxamides and identification of more stable class II histone deacetylase (HDAC) inhibitors. *Bioorg. Med. Chem. Lett.* **2008**, *18*, 6078−6082.
(52) Ontoria, J. M.; Altamura, S.; Di Marco, A.; Ferrigno, F.; Laufer, R.; Muraglia, E.; Palumbi, M. C.; Rowley, M.; Scarpelli, R.; Schultz-Fademrecht, C.; Serafini, S.; Steinkuhler, C.; Jones, P. Identification of novel, selective, and stable inhibitors of class II histone deacetylases. Validation studies of the inhibition of the enzymatic activity of HDAC4 by small molecules as a novel approach for cancer therapy. *J. Med. Chem.* **2009**, *52*, 6782−9.
(53) Patil, V.; Sodji, Q. H.; Kornacki, J. R.; Mrksich, M.; Oyelere, A. K. 3-Hydroxypyridin-2-thione as novel zinc binding group for selective histone deacetylase inhibition. *J. Med. Chem.* **2013**, *56*, 3492−506.
(54) Sodji, Q. H.; Patil, V.; Kornacki, J. R.; Mrksich, M.; Oyelere, A. K. Synthesis and Structure-Activity Relationship of 3-Hydroxypyridine-2-thione-Based Histone Deacetylase Inhibitors. *J. Med. Chem.* **2013**, *56*, 9969−9981.
(55) Ononye, S. N.; VanHeyst, M. D.; Oblak, E. Z.; Zhou, W.; Ammar, M.; Anderson, A. C.; Wright, D. L. Tropolones as lead-like natural products: the development of potent and selective histone deacetylase inhibitors. *ACS Med. Chem. Lett.* **2013**, *4*, 757−61.
(56) Wang, D.; Helquist, P.; Wiest, O. Zinc binding in HDAC inhibitors: a DFT study. *J. Org. Chem.* **2007**, *72*, 5446−9.
(57) Vanommeslaeghe, K.; Loverix, S.; Geerlings, P.; Tourwe, D. DFT-based ranking of zinc-binding groups in histone deacetylase inhibitors. *Bioorg. Med. Chem.* **2005**, *13*, 6070−82.
(58) McCarren, P.; Hall, M. L.; Whitehead, L. The Chemical Tuning of a Weak Zinc Binding Motif for Histone Deacetylase Using Electronic Effects. *Chem. Biol. Drug Des.* **2012**, *80*, 203−214.
(59) Vannini, A.; Volpari, C.; Filocamo, G.; Casavola, E. C.; Brunetti, M.; Renzoni, D.; Chakravarty, P.; Paolini, C.; De Francesco, R.; Gallinari, P.; Steinkuhler, C.; Di Marco, S. Crystal structure of a eukaryotic zinc-dependent histone deacetylase, human HDAC8, complexed with a hydroxamic acid inhibitor. *Proc. Natl. Acad. Sci. U. S. A.* **2004**, *101*, 15064−9.
(60) Waltregny, D.; de Leval, L.; Glenisson, W.; Tran, S. L.; North, B. J.; Bellahcene, A.; Weidle, U.; Verdin, E.; Castronovo, V. Expression of histone deacetylase 8, a class I histone deacetylase, is restricted to cells showing smooth muscle differentiation in normal human tissues. *Am. J. Pathol.* **2004**, *165*, 553−564.
(61) Estiu, G.; West, N.; Mazitschek, R.; Greenberg, E.; Bradner, J. E.; Wiest, O. On the inhibition of histone deacetylase 8. *Bioorg. Med. Chem.* **2010**, *18*, 4103−10.
(62) Dowling, D. P.; Gattis, S. G.; Fierke, C. A.; Christianson, D. W. Structures of metal-substituted human histone deacetylase 8 provide mechanistic inferences on biological function. *Biochemistry* **2010**, *49*, 5048−56.
(63) Singh, R. K.; Suzuki, T.; Mandal, T.; Balsubramanian, N.; Haldar, M.; Mueller, D. J.; Strode, J. A.; Cook, G.; Mallik, S.; Srivastava, D. K. Thermodynamics of Binding of Structurally Similar Ligands to Histone Deacetylase 8 Sheds Light on Challenges in the Rational Design of Potent and Isozyme-Selective Inhibitors of the Enzyme. *Biochemistry* **2014**, *53*, 7445−7458.
(64) Wu, R.; Lu, Z.; Cao, Z.; Zhang, Y. Zinc chelation with hydroxamate in histone deacetylases modulated by water access to the linker binding channel. *J. Am. Chem. Soc.* **2011**, *133*, 6110−3.
(65) Kunze, M. B.; Wright, D. W.; Werbeck, N. D.; Kirkpatrick, J.; Coveney, P. V.; Hansen, D. F. Loop interactions and dynamics tune the enzymatic activity of the human histone deacetylase 8. *J. Am. Chem. Soc.* **2013**, *135*, 17862−8.
(66) Chen, K.; Zhang, X.; Wu, Y. D.; Wiest, O. Inhibition and mechanism of HDAC8 revisited. *J. Am. Chem. Soc.* **2014**, *136*, 11636−43.
(67) Wu, R.; Wang, S.; Zhou, N.; Cao, Z.; Zhang, Y. A proton-shuttle reaction mechanism for histone deacetylase 8 and the catalytic role of metal ions. *J. Am. Chem. Soc.* **2010**, *132*, 9471−9.
(68) Wu, R.; Hu, P.; Wang, S.; Cao, Z.; Zhang, Y. Flexibility of Catalytic Zinc Coordination in Thermolysin and HDAC8: A Born-Oppenheimer ab initio QM/MM Molecular Dynamics Study. *J. Chem. Theory Comput.* **2009**, *6*, 337.
(69) Mysinger, M. M.; Carchia, M.; Irwin, J. J.; Shoichet, B. K. Directory of useful decoys, enhanced (DUD-E): better ligands and decoys for better benchmarking. *J. Med. Chem.* **2012**, *55*, 6582−94.
(70) Irwin, J. J.; Shoichet, B. K. ZINC−a free database of commercially available compounds for virtual screening. *J. Chem. Inf. Model.* **2005**, *45*, 177−82.
(71) Bruserud, O.; Stapnes, C.; Ersvaer, E.; Gjertsen, B. T.; Ryningen, A. Histone deacetylase inhibitors in cancer treatment: a review of the clinical toxicity and the modulation of gene expression in cancer cell. *Curr. Pharm. Biotechnol.* **2007**, *8*, 388−400.
(72) Erbe, D. V.; Wang, S.; Zhang, Y. L.; Harding, K.; Kung, L.; Tam, M.; Stolz, L.; Xing, Y.; Furey, S.; Qadri, A.; Klaman, L. D.; Tobin, J. F. Ertiprotafib improves glycemic control and lowers lipids via multiple mechanisms. *Mol. Pharmacol.* **2005**, *67*, 69−77.
(73) He, R.; Zeng, L. F.; He, Y.; Zhang, S.; Zhang, Z. Y. Small molecule tools for functional interrogation of protein tyrosine phosphatases. *FEBS J.* **2013**, *280*, 731−50.
(74) Vannini, A.; Volpari, C.; Gallinari, P.; Jones, P.; Mattu, M.; Carfi, A.; De Francesco, R.; Steinkuhler, C.; Di Marco, S. Substrate binding to histone deacetylases as shown by the crystal structure of the HDAC8-substrate complex. *EMBO Rep.* **2007**, *8*, 879−84.
(75) Whitehead, L.; Dobler, M. R.; Radetich, B.; Zhu, Y.; Atadja, P. W.; Claiborne, T.; Grob, J. E.; McRiner, A.; Pancost, M. R.; Patnaik, A.; Shao, W.; Shultz, M.; Tichkule, R.; Tommasi, R. A.; Vash, B.; Wang, P.; Stams, T. Human HDAC isoform selectivity achieved via exploitation of the acetate release channel with structurally unique small molecule inhibitors. *Bioorg. Med. Chem.* **2011**, *19*, 4626−34.
(76) Dowling, D. P.; Gantt, S. L.; Gattis, S. G.; Fierke, C. A.; Christianson, D. W. Structural studies of human histone deacetylase 8 and its site-specific variants complexed with substrate and inhibitors. *Biochemistry* **2008**, *47*, 13554−63.
(77) Zhang, Y.; Feng, J.; Jia, Y.; Wang, X.; Zhang, L.; Liu, C.; Fang, H.; Xu, W. Development of tetrahydroisoquinoline-based hydroxamic acid derivatives: potent histone deacetylase inhibitors with marked in vitro and in vivo antitumor activities. *J. Med. Chem.* **2011**, *54*, 2823−38.
(78) Jain, A. N. Surflex: fully automatic flexible molecular docking using a molecular similarity-based search engine. *J. Med. Chem.* **2003**, *46*, 499−511.
(79) Spitzer, R.; Jain, A. N. Surflex-Dock: Docking benchmarks and real-world application. *J. Comput.-Aided Mol. Des.* **2012**, *26*, 687−99.
(80) Pronk, S.; Pall, S.; Schulz, R.; Larsson, P.; Bjelkmar, P.; Apostolov, R.; Shirts, M. R.; Smith, J. C.; Kasson, P. M.; van der Spoel, D.; Hess, B.; Lindahl, E. GROMACS 4.5: a high-throughput and highly parallel open source molecular simulation toolkit. *Bioinformatics* **2013**, *29*, 845−54.
(81) Van Der Spoel, D.; Lindahl, E.; Hess, B.; Groenhof, G.; Mark, A. E.; Berendsen, H. J. GROMACS: fast, flexible, and free. *J. Comput. Chem.* **2005**, *26*, 1701−18.
(82) Lindorff-Larsen, K.; Piana, S.; Palmo, K.; Maragakis, P.; Klepeis, J. L.; Dror, R. O.; Shaw, D. E. Improved side-chain torsion potentials for the Amber ff99SB protein force field. *Proteins* **2010**, *78*, 1950−8.
(83) Webb, B.; Sali, A. Comparative Protein Structure Modeling Using MODELLER. *Curr. Protoc. Bioinf.* **2014**, *47*, 5 6 1−5 6 32.
(84) Cerutti, D. S.; Duke, R. E.; Darden, T. A.; Lybrand, T. P. Staggered Mesh Ewald: An extension of the Smooth Particle-Mesh Ewald method adding great versatility. *J. Chem. Theory Comput.* **2009**, *5*, 2322.
(85) Hess, B. P-LINCS: A parallel linear constraint solver for molecular simulation. *J. Chem. Theory Comput.* **2008**, *4*, 116−122.
(86) Schuttelkopf, A. W.; van Aalten, D. M. PRODRG: a tool for high-throughput crystallography of protein-ligand complexes. *Acta Crystallogr., Sect. D: Biol. Crystallogr.* **2004**, *60*, 1355−63.

DOI: 10.1021/ci500762z
J. Chem. Inf. Model. 2015, 55, 861−871

(87) Gordon, J. C.; Myers, J. B.; Folta, T.; Shoja, V.; Heath, L. S.; Onufriev, A. H++: a server for estimating pKas and adding missing hydrogens to macromolecules. *Nucleic Acids Res.* **2005**, *33*, W368−71.

DOI: 10.1021/ci500762z
J. Chem. Inf. Model. 2015, 55, 861−871